AIP Applied Physics Letters

Temperature dependence of terahertz optical characteristics and carrier transport dynamics in p-type transparent conductive CuCr1 x Mg x O2 semiconductor films

X. R. Li, M. J. Han, P. Chang, Z. G. Hu, Y. W. Li, Z. Q. Zhu, and J. H. Chu

Citation: Applied Physics Letters **104**, 012103 (2014); doi: 10.1063/1.4860994
View online: http://dx.doi.org/10.1063/1.4860994
View Table of Contents: http://scitation.aip.org/content/aip/journal/apl/104/1?ver=pdfcov
Published by the AIP Publishing

Temperature dependence of terahertz optical characteristics and carrier transport dynamics in *p*-type transparent conductive $CuCr_{1-x}Mg_xO_2$ semiconductor films

X. R. Li (李旭瑞), M. J. Han (韩美杰), P. Chang (常平), Z. G. Hu (胡志高),[a] Y. W. Li (李亚巍), Z. Q. Zhu (朱自强), and J. H. Chu (褚君浩)
Key Laboratory of Polar Materials and Devices, Ministry of Education, Department of Electronic Engineering, East China Normal University, Shanghai 200241, China

(Received 4 November 2013; accepted 16 December 2013; published online 2 January 2014)

Terahertz reflectance spectra and electrical transport of $CuCr_{1-x}Mg_xO_2$ films have been studied in temperature range of 150–300 K. With increasing temperature, the phonon mode near 15 THz shows a redshift trend, and free carrier absorption below 6 THz becomes more prominent. Moreover, hole effective mass increases linearly from 0.028 to 0.48 m_0 with the temperature and composition. Hall coefficient shows a turning-point at about 220, 206, and 194 K for the composition of $x = 0.02$, 0.06, and 0.10, respectively. The phenomena can be attributed to the transition of carrier transport mechanism from a thermal activation behavior to a variable range-hopping one. © *2014 AIP Publishing LLC*. [http://dx.doi.org/10.1063/1.4860994]

Transparent conducting oxide (TCO) semiconductors, which allow for fabricating "invisible electronic devices," are widely used in optoelectronic devices such as flat panel displays and photovoltaics.[1] Heretofore, most of TCOs such as impurity-doped ZnO, In_2O_3, and SnO_2 are *n*-type semiconductors.[2,3] However, many semiconductor applications, such as light emitting devices and transparent thin film transistors, are based on the principle of *p-n* junction. Thus, *p*-type TCOs have been paid much more attention in the past decades. Unfortunately, a higher resistivity and lower transparency compared to traditional *n*-type TCOs suggest that there are still some key challenges in producing high-quality *p*-type TCOs.[4] Recently, delafossite-structured ABO_2 oxides become the important issue as a potential candidate for *p*-type TCOs due to the pioneer work on transparent $CuAlO_2$ conductive film.[5] Correspondingly, some other isostructural delafossite materials like $CuCrO_2$ and $CuGaO_2$ films have also been reported.[6] Among these delafossite-structured ABO_2 systems, it was found that $CuCr_{0.95}Mg_{0.05}O_2$ film prepared by radio frequency sputtering has the lowest resistivity of 0.0045 Ω cm without post-annealing, which shows a promising *p*-type TCO semiconductor for fabricating optoelectronic devices. However, its transparency in the visible range is only about 30%, which is much less than those of traditional *n*-type TCOs. It was claimed that the transparency can be improved by annealing at high temperatures, but with a consequence of the enormous increase in electrical resistivity.[7,8] In addition, the resistivity of $CuCr_{1-x}Mg_xO_2$ has also been discussed as a basic physical parameter.[9] It was found that there is the turning point for the temperature dependent behavior. Nevertheless, the physical mechanism and origin have not been clarified due to the limited experimental data.

Following the above concept, we prepared $CuCr_{1-x}Mg_xO_2$ nanocrystalline films by the sol-gel route, which have been proved to possess relatively high transmittance (above 70%) in the visible-near-infrared wavelength region.[10] It was found that the $CuCr_{0.9}Mg_{0.1}O_2$ film has a relatively low resistivity of about 0.34 Ω cm at room temperature. Moreover, the films are of good electrical stability even at high temperatures because the high-temperature synthetic procedure has already been included during the annealing process.[10,11] However, other interesting electrical parameters such as carrier concentration and mobility of $CuCr_{1-x}Mg_xO_2$ films have not been presented well to date. As for the transparency of TCOs, people usually focus on whether the band gap is wide enough for the excitations in the visible region. It was reported that the free-carrier absorption (FCA) effect should also be considered while designing TCO layers for devices because it introduces an additional absorption source, which limits the optical transparency.[3] On the other hand, terahertz (THz) optical properties for these films have greatly guiding significance for fabricating optoelectronic devices, which have not been carried out. By analyzing the THz characteristics, one can determine the optical response for the free carriers because the FCA effect usually plays an important role in low THz-frequency region.[3,12] The key parameters like photoelectric conversion efficiency for devices can be determined and improved by controlling the carrier dynamics of the $CuCr_{1-x}Mg_xO_2$ films. Therefore, the free carrier properties are required for clarifying these physical mechanisms and evaluating prototype device performance. In this Letter, THz reflectance spectra and Hall transport measurements of sol-gel derived $CuCr_{1-x}Mg_xO_2$ films at different temperatures have been carried out to study carrier concentration and mobility.

The $CuCr_{1-x}Mg_xO_2$ ($x = 0.02$, 0.06, and 0.10) films were prepared on (001) sapphire substrates by the sol-gel route employing a spin-coating process. A detailed fabrication procedure can be found in Ref. 10. The THz reflectance spectra were recorded by a Bruker Vertex 80 V Fourier Transform infrared (FT-IR) spectrometer equipped with a specular reflectance setup. The externally incident angle was

[a]Author to whom correspondence should be addressed. Electronic mail: zghu@ee.ecnu.edu.cn. Tel.: +86-21-54345150. Fax: +86-21-54345119.

set to about 10°. The spectra were measured in the frequency range of 1.5–18 THz with a resolution of 0.06 THz (i.e., 50–600 cm^{-1}). The film was mounted into an Oxford Optistat AC-V12w continuous flow cryostat with the film in He vapor. The experimental temperature region can be varied from 150 to 300 K. On the other hand, temperature dependent Hall-effect measurements were done by a home-build system, which is based on an Oxford Spectromag SM4000 magnetic system equipped with a series of precise electrical instruments: the current source (Keithley 6221), the digital nanovoltmeter (Keithley 2182 A), the switch mainframe (Keithley 7001) with a Hall-effect card (Keithley 7065) inside. In addition, the sub-femtoamp remote sourcemeter (Keithley 6430) was used as a supplement for high-resistance measurements.

One of the critical concerns for optoelectronic device design is the interaction between free carriers and photons in the THz region. Since the reststrahlen region of sapphire overlaps with those of $CuCr_{1-x}Mg_xO_2$, it is difficult to identify the phonon frequencies directly from the measured reflectance spectra. A three-phase model (air/film/substrate) was used to calculate the reflectance spectra of the $CuCr_{1-x}Mg_xO_2$ films.[12] A Lorentz-Drude dielectric function model was presented to explain the experimental reflectance data. The complex THz dielectric functions ($\tilde{\varepsilon} = \varepsilon_1 + i\varepsilon_2$) of the $CuCr_{1-x}Mg_xO_2$ films can be written as $\tilde{\varepsilon} = \varepsilon_\infty + S\omega_{TO}^2/(\omega_{TO}^2 - \omega^2 - i\omega\Gamma) - \varepsilon_\infty\omega_p^2/(\omega^2 + i\omega\gamma)$. Here, $\varepsilon_\infty, \omega_{TO}$, S, Γ, ω_p, and γ represent, in order, the high-frequency dielectric constant, transverse-optical (TO) phonon frequency, the oscillator strength, the broadening value of TO phonon, the plasma frequency, and the phenomenological damping constant, respectively. The experimental reflectance spectra of the sapphire substrate at different temperatures have been fitted using the Lorentz model without the Drude item. The phonon modes near 11.5, 13.2, and 17.1 THz belong to the vibration from the sapphire substrate.[12] These fitting parameters from the sapphire substrate were used for reproducing the reflectance spectra of the $CuCr_{1-x}Mg_xO_2$ films with the composition x from 0.02 to 0.10 at different temperatures. For instance, the experimental data (circles) and fitting data (solid lines) at the lowest temperature of 150 K, the middle temperature of 225 K and the highest temperature of 300 K are shown in Fig. 1(a). A good agreement between the experimental and calculated spectra can be found over the entirely experimental frequency region. The best fitting parameter values together with the error bars are listed in Table I.

Group-theoretical analysis decomposes a general mode for delafossite oxide $CuMO_2$ (M = trivalent cation) at the Brillouin zone center as: $\Gamma = A_{1g} + E_g + 3A_{2u} + 3E_u$.[11,13,14] The observed infrared active modes near 15 THz (about 500 cm^{-1}) can be inferred to the Eu ↑ vibration. The experimental reflectance spectra of the $CuCr_{0.94}Mg_{0.06}O_2$ film between 14.9 and 15.4 THz at different temperatures are shown in Fig. 1(b). As we can see, the phonon band becomes broadening and its intensity decreases with increasing temperature. From Table I, the derived carrier concentration increases with the temperature. Thus, with increasing temperature, the LO-phonon plasmon (LPP) coupling effect becomes more evident and separates the unscreened LO phonon and plasma frequencies into modes with different energies.[15] It can also be found that the peak center of the

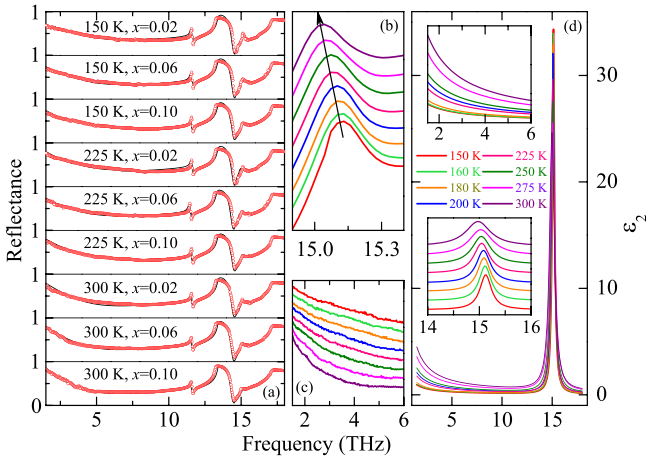

FIG. 1. (a) Experimental THz reflectance spectra (circles) and best-fit results (solid lines) for the $CuCr_{1-x}Mg_xO_2$ films at the temperature of 150 K, 225 K, and 300 K, respectively. (b) Experimental reflectance spectra of the $CuCr_{0.94}Mg_{0.06}O_2$ film between 14.85 and 15.35 THz at different temperatures. (c) An enlarged reflectance spectral region at frequency below 6 THz from $CuCr_{0.94}Mg_{0.06}O_2$ film. (d) The imaginary part of THz dielectric functions for the $CuCr_{0.9}Mg_{0.1}O_2$ film at different temperatures. The upper inset of (d) shows the detail of the imaginary part between 1.5 and 6 THz, while the lower one shows the detail of the frequency in the range of 14–16 THz.

Eu ↑ mode shifts to a lower frequency with increasing temperature, which is mainly caused by the lattice thermal expansion. The anharmonic phonon-phonon interactions become more important as the temperature increases owing to the increase of statistical number of acoustic phonons, which also induces the redshift of the phonon mode.[16]

The imaginary part ε_2 of the complex THz dielectric functions from the $CuCr_{0.9}Mg_{0.1}O_2$ film at different temperatures is shown in Fig. 1(d). The imaginary part becomes slightly larger with increasing temperature over the entire frequency region, which means that lower temperature can result in a higher transparency. The imaginary part of the complex dielectric functions increases with decreasing frequency in the low frequency region, indicating that the THz absorption coefficient increases with decreasing light frequency. This is due to the FCA effect, which is an important phenomenon in semiconductor materials.[12,17] The increasing tendency in low THz frequency region becomes more obvious with increasing temperature, suggesting that the FCA becomes stronger with the temperature. This is because the carrier concentration increases with the temperature, as will be discussed in the following. The higher carrier concentration can lead to larger free carrier absorption.[18] Moreover, the FCA can be observed directly from the reflectance spectra in the low frequency region, as shown in Fig. 1(c). However, the decreasing tendency with increasing frequency gradually disappears in the frequency region beyond 6 THz. The data agree well with the observed phenomena in the visible-near-infrared region.[10] It manifests that the FCA can be negligible and causes little optical loss even for the $CuCr_{1-x}Mg_xO_2$ films at high carrier concentrations above the frequency of 6 THz.

Let us shed light on the electrical parameters varied with the temperature. The resistivity ρ increases with the temperature and the lowest resistivity for the films at room

TABLE I. Lorentz oscillator and Drude parameter values at different temperatures are taken from the best fit to THz reflectance spectra of the $CuCr_{1-x}Mg_xO_2$ films. The 90% confidence limits of the fitting parameters are given in parentheses. The hole concentration (p) was determined from the Hall-effect measurements. The hole effective mass m^* is in the ration of m_0 (here, m_0 is the mass of the free electron).

Composition (x)	Temperature (K)	p (cm^{-3})	ε_∞	S	ω_{TO} (cm^{-1})	Γ (cm^{-1})	ω_p (cm^{-1})	γ ($\times 10^5$ cm^{-1})	m^* (m_0)
0.02	300	1.16×10^{17}	5.63	0.62	500.6	13.3	211	2.21	0.042
			(0.10)	(0.01)	(0.3)	(0.6)	(3)	(0.03)	
	250	2.70×10^{16}	5.59	0.67	501.4	10.7	104	1.26	0.040
			(0.10)	(0.05)	(0.5)	(0.3)	(4)	(0.02)	
	200	7.74×10^{15}	5.55	0.72	502.4	9.0	63	1.17	0.032
			(0.12)	(0.02)	(0.2)	(0.6)	(3)	(0.04)	
	150	2.18×10^{15}	5.49	0.79	504.5	5.8	36	0.95	0.028
			(0.10)	(0.04)	(0.3)	(0.8)	(4)	(0.01)	
0.06	300	2.04×10^{19}	5.89	0.56	500.0	13.4	921	4.52	0.46
			(0.01)	(0.03)	(0.1)	(0.4)	(10)	(0.01)	
	250	1.47×10^{19}	5.81	0.58	501.0	9.0	819	5.63	0.42
			(0.01)	(0.02)	(0.5)	(0.3)	(12)	(0.01)	
	200	8.62×10^{18}	5.81	0.62	502.2	6.5	656	9.71	0.39
			(0.02)	(0.09)	(0.2)	(0.9)	(13)	(0.02)	
	150	5.48×10^{18}	5.70	0.70	504.4	6.0	546	18.01	0.36
			(0.04)	(0.05)	(0.5)	(0.8)	(6)	(0.02)	
0.10	300	3.40×10^{20}	6.33	0.39	500.4	23.7	2248	4.34	0.48
			(0.10)	(0.01)	(0.2)	(0.6)	(43)	(0.02)	
	250	2.21×10^{20}	6.29	0.42	501.6	14.5	1870	7.43	0.32
			(0.10)	(0.05)	(0.3)	(0.3)	(87)	(0.07)	
	200	1.16×10^{20}	6.27	0.45	502.9	11.00	1383	11.17	0.23
			(0.12)	(0.02)	(0.6)	(0.6)	(32)	(0.02)	
	150	7.36×10^{19}	6.23	0.55	504.7	9.0	1126	18.94	0.15
			(0.10)	(0.04)	(0.3)	(0.8)	(35)	(0.02)	

temperature is 39.5, 0.49, and 0.47 Ω cm with increasing Mg composition, respectively. From Fig. 2(a), we can see that temperature dependence of the resistivity shows a turning-point at a special temperature point (T_{cross}). In the temperature region from 300 K to T_{cross}, the plot of lnρ *vs.* 1000/T shows a linear change because the carrier transport mechanism obeys a thermal activation behavior. The parameter $1/\rho$ is in proportion to $A\exp(-E_a/k_BT)$, where E_a is the thermal activation energy, k_B is Boltzmann constant, and A is a constant.[19] Below T_{cross}, the carrier transport obeys a three-dimensional variable range hopping (VRH) mechanism, since the lnρ is proportional to $(1/T)^{1/4}$.[9] The plot lnρ *vs.* $(1/T)^{1/4}$ shows a linear relationship, as shown in Fig. 2(b). The parameter T_{cross} for the films with the composition of $x = 0.02$, 0.06, and 0.10 is estimated to be 220 ± 10 K, 206 ± 10 K, and 194 ± 10 K, respectively. It can be concluded that the parameter T_{cross} drops with increasing composition x. It is because the substitution at the Cr^{3+} site by the Mg^{2+} ion disturbs the spin fluctuation of the local spin at Cr sites at a lower temperature. Moreover, the disturbance becomes stronger with increasing Mg doping.

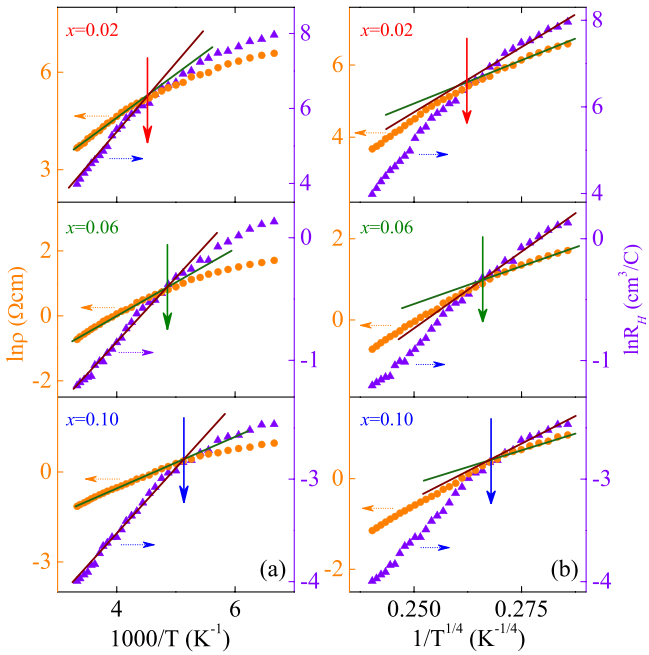

FIG. 2. (a) The functions of lnρ *vs.* 1000/T and lnR_H *vs.* 1000/T are shown by dots and triangles for the $CuCr_{1-x}Mg_xO_2$ films, respectively. (b) The functions of lnρ *vs.* $(1/T)^{1/4}$ and lnR_H *vs.* $(1/T)^{1/4}$ are shown by dots and triangles, respectively. Note that the solid lines show the linear fitting and the vertical arrows indicate the turning-point temperatures.

The Hall coefficient R_H under different temperatures for the $CuCr_{1-x}Mg_xO_2$ films has been recorded at low magnetic fields below 2 T. The positive value of R_H demonstrates that $CuCr_{1-x}Mg_xO_2$ is a p-type semiconductor and the Hall coefficient decreases with increasing temperature. Surprisingly, the temperature dependent R_H also shows a turning-point at nearly the same temperature as the resistivity does. It means that the carrier transport mechanism makes a great contribution to the Hall coefficient for the $CuCr_{1-x}Mg_xO_2$ films. For temperature above T_{cross}, the plots of ln R_H *vs.* 1000/T show a linear variation as the normal-state transport.[20] For temperature below T_{cross}, however, it shows a more complex trend. As shown in Fig. 2(b), one can see an approximate linearity from ln R_H *vs.* $(1/T)^{1/4}$, suggesting that the R_H is in

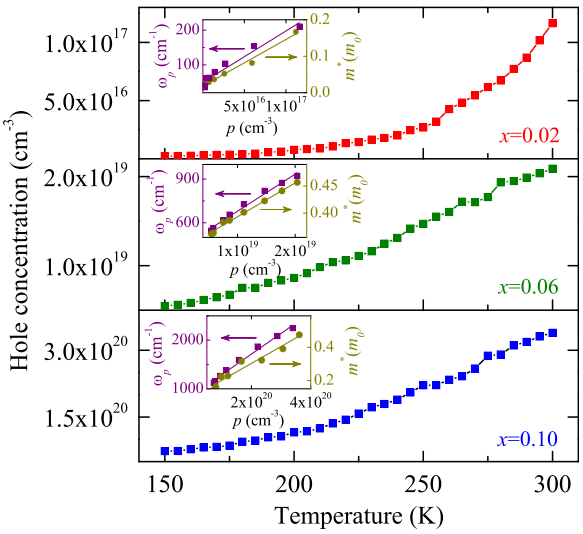

FIG. 3. The carrier concentration is varied with the temperature for the $CuCr_{1-x}Mg_xO_2$ films. The insets show that the plasma frequency and the effective mass increase linearly with the hole concentrations for three Mg composition, respectively.

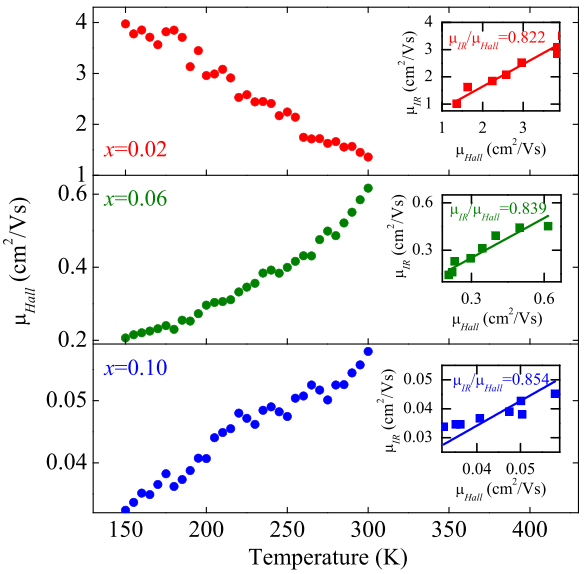

FIG. 4. Temperature dependence of the Hall mobility for the $CuCr_{1-x}Mg_xO_2$ films. The insets show the comparison between the Hall mobility and infrared mobility for different Mg compositions, respectively.

three-dimensional variable range hopping region.[21] The hole concentration, which can be estimated from the Hall coefficient: $p = 1/(R_H e)$ (here, e is the electron charge), increases with the temperature (Fig. 3). At lower temperatures, the hole concentration increases slightly with the temperature. As the temperature goes up, the tendency becomes more striking. The increasing hole concentration with the temperature mainly results from the partly ionized impurity.[22] It can be found that the $CuCr_{0.98}Mg_{0.02}O_2$ film is still located in the partly ionized region near room temperature. Meanwhile, the films with higher doping concentrations ($x = 0.06$ and 0.10) have been already approaching the fully ionized region, where semiconductor devices usually work. It indicates that the heavily doped $CuCr_{1-x}Mg_xO_2$ is a very potential TCO material for room-temperature device. This is because with increasing doping concentration, the inducing defects increase in the top of the valence-band, which results in the form of the tail states in this band. In addition, the band-gap renormalization (BGR) effect raises the energy of the highest valence-band maximum. Our previous works have proved that the $CuCr_{0.98}Mg_{0.02}O_2$ film has the largest direct band gap of 3.11 eV at room temperature. When the Mg composition increases from 0.02 to 0.06, the hole concentration is increased from 1.3×1017 to 2.1×10^{19} cm^{-3}, which induces that the direct band gap rapidly declines to 3.00 eV.[10] The band-gap shrinkage (about 0.1 eV) suggests that the electronic transition energies decrease with increasing Mg composition.[23] Thus, the relationship between the hole concentration and the BGR effect for heavily doped $CuCr_{1-x}Mg_xO_2$ semiconductor is an essential factor to be considered for device designing.

Temperature dependent Hall mobility ($\mu_{Hall} = R_H/\rho$) of the films are plotted in Fig. 4. The mobility of the $CuCr_{0.98}Mg_{0.02}O_2$ film increases from 1.358 to 3.973 cm^2/(V s) with the temperature, while the mobility of the $CuCr_{0.94}Mg_{0.06}O_2$ and $CuCr_{0.90}Mg_{0.10}O_2$ films decreases with increasing temperature. This is attributed to different dominant scattering mechanism. For doping semiconductor materials, the ionized impurity scattering time increases with the temperature, while the lattice vibration scattering time decreases with increasing temperature. In addition, for ionized impurity scattering mechanism, the scattering time is in proportion to the impurity concentration.[22,24] As shown in Table I, the hole scattering time decreases with increasing temperature for the $CuCr_{0.98}Mg_{0.02}O_2$ film. This is because the lattice vibration predominates the scattering mechanism, and the impurity concentration is too low for ionized impurity scattering mechanism to take obvious effect. With increasing doping concentrations, the effect of ionized impurity scattering mechanism becomes more important. Thus, the total scattering time increases with the temperature for the other two compositions. On the other hand, the mobility can also be calculated from the damping constant γ and the hole effective mass m^* by $\mu = e/(2\pi c m^* \gamma)$. Here, m^* is the hole effective mass and can be calculated using the formula: $\omega_p = \sqrt{(pe^2)/(\varepsilon_0 \varepsilon_\infty m^*)}$, where ε_0 is the vacuum permittivity, p is the hole concentrations obtained from the Hall-effect measurements. The damping constant γ and plasma frequency ω_p can be taken from the best-fit parameters in Table I. The ω_p increases with the temperature and Mg composition, indicating that it increases with the hole concentrations. For example, the m^* for the Mg composition of 0.02 increases from 0.028 to 0.042 m_0 and from 0.15 to 0.48 m_0 for the Mg composition of 0.1, respectively. The hole effective mass increases with the temperature, which agrees with the typical semiconductors reported previously.[25] Finally, the comparison between the Hall mobility μ_{Hall} and the optical mobility μ_{IR} is presented in the insets of Fig. 4. The average ratio (μ_{IR}/μ_{Hall}) is estimated to be 0.822, 0.839, and 0.854 with increasing Mg composition, repectively. In most cases, the optical mobility tends to be slightly less than Hall mobility, as mentioned in the earlier reports.[26,27] Nevertheless, the μ_{IR}/μ_{Hall} ratio above 0.8 can be reasonably acceptable within the error range. It indicates that the electrical parameters derived from spectral and transport analyses are reasonable and reliable.

In summary, the imaginary part of the complex THz dielectric functions from $CuCr_{1-x}Mg_xO_2$ films increases with decreasing frequency due to the FCA effect. The change of the carrier transport mechanism from a thermal activation behavior to a variable range-hopping one causes the appearance of turning-point for Hall coefficient.

This work was financially supported by Major State Basic Research Development Program of China (Grant Nos. 2011CB922200 and 2013CB922300), Natural Science Foundation of China (Grant Nos. 11374097, 61376129, 11074076, and 61106122), Projects of Science and Technology Commission of Shanghai Municipality (Grant Nos. 13JC1402100 and 13JC1404200), and the Program for Professor of Special Appointment (Eastern Scholar) at Shanghai Institutions of Higher Learning.

[1]T. Minami, Semicond. Sci. Technol. **20**, S35 (2005).
[2]J. F. Li, L. B. Hu, J. Liu, L. Wang, T. J. Marks, and G. Grüner, Appl. Phys. Lett. **93**, 083306 (2008).
[3]H. Peelaers, E. Kioupakis, and C. G. Van de Walle, Appl. Phys. Lett. **100**, 011914 (2012).
[4]E. Arca, K. Fleischer, and I. V. Shvets, Appl. Phys. Lett. **99**, 111910 (2011).
[5]H. Kawazoe, M. Yasukawa, H. Hyodo, M. Kurita, H. Yanagi, and H. Hosono, Nature **389**, 939 (1997).
[6]M. J. Han, K. Jiang, J. Z. Zhang, W. L. Yu, Y. W. Li, Z. G. Hu, and J. H. Chu, J. Mater. Chem. **22**, 18463 (2012).
[7]R. Nagarajan, A. D. Draeseke, A. W. Sleight, and J. Tate, J. Appl. Phys. **89**, 8022 (2001).
[8]Y. F. Wang, Y. J. Gu, T. Wang, and W. Z. Shi, J. Alloys Compd. **509**, 5897 (2011).
[9]T. Okuda, N. Jufuku, S. Hidaka, and N. Terada, Phys. Rev. B **72**, 144403 (2005).
[10]M. J. Han, Z. H. Duan, J. Z. Zhang, S. Zhang, Y. W. Li, Z. G. Hu, and J. H. Chu, J. Appl. Phys. **114**, 163526 (2013).
[11]M. J. Han, K. Jiang, J. Z. Zhang, Y. W. Li, Z. G. Hu, and J. H. Chu, Appl. Phys. Lett. **99**, 131104 (2011).
[12]Z. G. Hu, M. Strassburg, N. Dietz, A. G. U. Perera, A. Asghar, and I. T. Ferguson, Phys. Rev. B **72**, 245326 (2005).
[13]S. P. Pavunny, A. Kumar, and R. S. Katiyar, J. Appl. Phys. **107**, 013522 (2010).
[14]J. Pellicer-Porres, A. Segura, E. Martínez, A. M. Saitta, A. Polian, J. C. Chervin, and B. Canny, Phys. Rev. B **72**, 064301 (2005).
[15]Z. G. Hu, M. B. M. Rinzan, S. G. Matsik, A. G. U. Perera, G. Von Winckel, A. Stintz, and S. Krishna, J. Appl. Phys. **97**, 093529 (2005).
[16]T. D. Kang, E. C. Standard, P. D. Rogers, K. H. Ahn, and A. A. Sirenko, Phys. Rev. B **86**, 144112 (2012).
[17]S. M. Harrel, R. L. Milot, J. M. Schleicher, and C. A. Schmuttenmaer, J. Appl. Phys. **107**, 033526 (2010).
[18]H. M. Ali, H. A. Mohamed, M. M. Wakkad, and M. F. Hasaneen, Thin Solid Films **515**, 3024 (2007).
[19]D. Li, X. Fang, A. Zhao, Z. Deng, W. Dong, and R. Tao, Vacuum **84**, 851 (2010).
[20]A. Carrington, A. P. Mackenzie, C. T. Lin, and J. R. Cooper, Phys. Rev. Lett. **69**, 2855 (1992).
[21]T. Klein, P. Achatz, J. Kacmarcik, C. Marcenat, F. Gustafsson, J. Marcus, E. Bustarret, J. Pernot, F. Omnes, B. E. Sernelius, C. Persson, A. Ferreira da Silva, and C. Cytermann, Phys. Rev. B **75**, 165313 (2007).
[22]S. S. Li, *Semiconductor Physical Electronics*, 2nd ed. (Springer, New York, 2006).
[23]A. Walsh, J. L. F. Da Silva, and S.-H. Wei, Phys. Rev. B **78**, 075211 (2008).
[24]D. B. M. Klaassen, Solid State Electrons **35**, 961 (1992).
[25]M. A. Green, J. Appl. Phys. **67**, 2944 (1990).
[26]W. Songprakob, R. Zallen, W. K. Liu, and K. L. Bacher, Phys. Rev. B **62**, 4501 (2000).
[27]Y. C. Chen, S. H. Li, P. K. Bhattacharya, J. Singh, and J. M. Hinckley, Appl. Phys. Lett. **64**, 3110 (1994).